A&A manuscript no.
(will be inserted by hand later)

Your thesaurus codes are:
08(10.03.1; 13.09.3; 13.09.4; 09.13.2; 09.03.1; 09.04.1)

ASTRONOMY AND ASTROPHYSICS

arXiv:astro-ph/0002478v1 25 Feb 2000

Non-equilibrium H_2 ortho-to-para ratio in two molecular clouds of the Galactic Center⋆

N.J. Rodríguez-Fernández[1], J. Martín-Pintado[1], P. de Vicente[1], A. Fuente[1], S. Hüttemeister[2], T.L. Wilson[3,4], and D. Kunze[5]

[1] Observatorio Astronómico Nacional (IGN), Apartado 1143, E-28800, Alcalá de Henares, Spain (nemesio, martin, vicente, fuente@oan.es)
[2] Astronomische Institute, Auf dem Huegel 71, D-53121 Bonn 1, Germany (huette@astro.uni-bonn.de)
[3] Max–Planck Institut für Radioastronomie, Postfach 2024, D 53010 Bonn,
[4] Sub-mm Telescope Observatory, Steward Observatory, The University of Arizona, Tucson, Az, 85728, USA (twilson@as.arizona.edu)
[5] MPE, Giesenbachstrasse 1, D-85748 Garching, Germany (kunze@mpe.mpg.de)

Received date; accepted date

Abstract. We present ISO observations of the S(0), S(1), S(2), and S(3) rotational lines of molecular hydrogen from two molecular clouds near the Galactic Center (GC). We have also measured continuum dust emission at infrared wavelengths with ISO and the rotational radio lines J=1–0 of ^{13}CO and C^{18}O and J=2–1 of C^{18}O with the IRAM-30m telescope. Using the dust continuum spectra and the CO lines we derive a total visual extinction of $\sim$ 15-20 magnitudes toward these GC clouds. After correcting the H_2 data for extinction, the gas temperatures are $\sim$ 250 K and the column densities of warm gas are $\sim 2\times10^{21}$ cm^{-2}. This is the first direct measure of the H_2 column densities of the warm component; with this, we estimate an NH_3 abundance in the warm gas of $\sim$ 2 10^{-7}. The column density of warm gas is, at least, a factor of 100 larger than the corresponding column densities derived from the warm dust. The observed ortho-to-para ratio (OTPR) is $\sim$ 1, clearly below the local thermodynamical equilibrium (LTE) OTPR for gas at 250 K of $\sim$ 3. Low velocity shocks ($\sim$ 10 km s^{-1}) are the most likely explanation for the column densities of warm gas and dust and the non-LTE H_2 OTPR.

Key words: ISM: clouds – ISM: molecules – ISM: dust, extinction – Galaxy: center – Infrared: ISM: continuum – Infrared: ISM: lines and bands

1. Introduction

The central $\sim 6^\circ$ of our galaxy exhibit a large accumulation of molecular material which is forming big molecular clouds whose masses and sizes are so large as 10^6 $M_\odot$ and 15 pc, respectively. These clouds are denser (average densities of 10^4 cm^{-3}), more turbulent (line widths of $\sim$ 20 km s^{-1}), and hotter (with a warm component with temperatures, T, up to 200-300 K) than the clouds of the disk of the galaxy (see e.g. Morris & Serabyn 1996). The high temperatures in Galactic Center (GC) clouds were known basically by observations of NH_3 inversion lines over limited regions (Güsten et al. 1981; Mauersberger et al. 1986). Hüttemeister et al. (1993) analyzed 36 molecular clouds distributed all along the Central Molecular Zone and the "Clump 2" complex; they showed that high kinetic temperatures are a general characteristic of the GC clouds and not only of those located close to Sgr A and Sgr B2. In the disk of the galaxy, kinetic temperatures higher than 100 K are associated with infrared sources, that is, embedded stars which heat the dust and subsequently the gas by collisions with the dust grains. The typical sizes of such regions are less than 1 pc. The high kinetic temperatures in the GC clouds are found in regions of $\sim$ 10 pc, where one measures large column densities of cold dust ($T < 30$ K, Odenwald & Fazio 1984; Cox & Laureijs 1989). This rules out gas-dust collisions as a possible heating mechanism of the warm component. Dissipation of turbulence due to shocks induced by the rotation of the galaxy could be the main heating mechanism in the GC clouds (Wilson et al. 1982).

Unfortunately the NH_3 abundance in the warm component was unknown since one could not estimate the warm H_2 column densities. The *Infrared Space Observatory* (ISO; Kessler et al. 1996), has allowed us, for the first time, to measure directly the total column density of warm gas by observing pure-rotational lines of H_2. These trace gas with temperatures of a few hundreds Kelvin. ISO has also allowed us to study the H_2 ortho-to-para ratio (OTPR), which can help determine the possible heating

⋆ ISO is an ESA project with instruments funded by ESA Member States (especially the PI countries: France, Germany, the Netherlands and the United Kingdom) and with the participation of ISAS and NASA.

mechanism and the origin of this molecule. Before ISO, the H_2 OTPR had been studied in regions with temperatures of $\sim$ 2000 K, using the vibrational lines. In such shock-excited sources, one measures an OTPR of $\sim$ 3 (Smith et al. 1997), which is the local thermodynamical equilibrium (LTE) value for $T \gtrsim$ 200 K. In contrast, for regions heated mainly by ultraviolet (UV) radiation (Photodissociation regions [PDRs]), the vibrational lines give OTPRs in the range of 1.2-2 (see e.g. Chrysostomou et al. 1993). However, these low OTPRs might not be a consequence of an actual non-LTE ortho-to-para *abundances* ratio but a result of optical depth effects in the fluorescence-pumping of the ortho-H_2 (Sternberg & Neufeld 1999). Using these considerations, one can explain why the PDR in S140 exhibits an OTPR $\sim$ 2 in the vibrational states but 3 in the lowest rotational levels.

There are two cases of non-equilibrium OTPR measured from the pure-rotational lines: the shock excited source HH54 (Neufeld et al. 1998) and the PDR associated with the reflection nebula NGC 7023 (Fuente et al. 1999). The first case has been explained using the shocks model of Timmermann (1998), which involves transient heating by low velocity shocks. To explain the non-LTE OTPR in NGC 7023, it was necessary to invoke a dynamic dissociation front.

To investigate the thermal balance of the GC clouds we have selected 18 clouds from the samples of Hüttemeister et al. (1993) and Martín-Pintado et al. (1997) and we have observed them with the ISO satellite. In this paper we present H_2 observations toward two sources which show similar characteristics (also shown in the NH_3 studies of Hüttemeister et al. 1993), indicating that their heating mechanisms are also very similar. In particular, they show a non-LTE OTPR. The detection of OTPRs out of equilibrium in the GC clouds gives us new insights into the heating mechanism, since the gas must be heated to several hundreds K almost without changing the OTPR of cold gas.

In Sects. 2 and 3, we present observations and results, respectively, and in Sect. 4 we discuss the possible heating mechanism and the origin of the non-equilibrium OTPR.

2. Observations and data reduction

2.1. ISO observations

We observed the pure-rotational H_2 lines S(0), S(1), S(2), and S(3) with the *Short Wavelength Spectrometer* (SWS; de Graauw et al. 1996) on board ISO toward two molecular clouds. The galactic coordinates and ISO beam sizes are given in Table 1. These sources are among the farthest from the dynamical center of the galaxy in our sample. M+3.06+0.34 [α(2000)= $17^h\ 51^m\ 26\overset{s}{.}4$, δ(2000) = -26°08′29″.4] is located in the "Clump 2" complex (Stark & Bania 1986), while M+1.56−0.30 [α(2000)= $17^h\ 50^m\ 26\overset{s}{.}6$, δ(2000) = -27°45′29″.5] belongs to the "l=1°.5-complex" (Bally et al. 1988). The observations were made during orbits 313 (S(0) and S(3) lines), and 467 (S(1) and S(2) lines). The wavelength bands were scanned in the SWS02 mode with a typical on-target time of 100 s. The spectral resolution ($\lambda/\Delta\lambda$) of this mode is $\sim$ 1000-2000 corresponding to a velocity resolution of $\sim$ 150-300 km s^{-1} . All the lines have broader profiles than those expected for a point source by a factor 1.3-1.5, indicating that the sources are extended in the direction perpendicular to the slit (see Valentijn & Van der Werf 1999). The flux calibration is believed to be accurate to 30%, 20%, 25%, and 25% for the S(0), S(1), S(2), and S(3) lines, respectively (Salama et al. 1997). Data reduction was carried out with version 6 of the SWS Interactive Analysis at the ISO Spectrometer Data Center at MPE. Further analysis has been made using the ISAP [1] software package. All lines have been rebinned to one fifth of the spectral resolution of the instrument. Fig. 1a-b shows the spectra, and the observed parameters are given in Table 1. The errors in the radial velocities of the H_2 lines listed in this table have been estimated from the Gaussian fits. The wavelength calibration uncertainties, expressed in velocities, are typically of 20-40 km s^{-1} for $\lambda > 12\mu$m and $\sim$ 25-60 km s^{-1} for $\lambda < 12\mu$m (Valentijn et al. 1996). Thus, the calibration uncertainties usually dominate the global error in the radial velocities. When one takes into account the errors from the Gaussian fits and the wavelength calibration uncertainties, the central velocities of the H_2 lines are in agreement with those measured from the CO lines (section 2.2). It is noteworthy that, the higher the signal-to-noise ratio of the H_2 lines (S(1) lines), the better the agreement of the H_2 radial velocities with those of CO.

We also present *Long Wavelength Spectrometer* (LWS; Clegg et al. 1996; Swinyard et al. 1996) observations of these sources in grating mode (43-196.7 μm, $\lambda/\Delta\lambda \sim 200$). Fig. 1 e-f shows the LWS spectra. The spectral resolution was 0.29 μm for the 43-93 μm range and 0.6 μm for the 80-196 μm range. The LWS aperture was $\sim 80" \times 80"$. The roll angle, which gives the orientation of the apertures, was 90°± 2°for both the SWS and the LWS observations. Data were taken during orbits 315 and 318 and processed through the LWS Pipeline Version 7. The individual detector scans were calibrated to within 10% of each other, based on overlapping detectors. Post-pipeline analysis (including shifting the different detectors using dark currents and defringing) was performed with ISAP.

2.2. IRAM 30-m observations

The J=1–0 line of ^{13}CO and C^{18}O and the J=2–1 line of C^{18}O were observed simultaneously with the IRAM 30-m

[1] The ISO Spectral Analysis Package (ISAP) is a joint development by the LWS and SWS Instrument Teams and Data Centers. Contributing institutes are CESR, IAS, IPAC, MPE, RAL and SRON.

telescope (Pico Veleta, Spain) in May 1997. We used two SIS receivers at 3 and 1.3 mm connected to two 512×1 MHz channel filter banks. This configuration provided a velocity resolution of 2.7 and 1.4 km s^{-1} for the J=1–0 and J=2–1 lines respectively. Typical system temperatures were $\sim$ 250 K for the J=1–0 line and $\sim$ 500 K for the J=2–1 line. The receivers were tuned to single side band with rejections always larger than 10 dB that were checked against standard calibration sources. The beam size of the 30-m telescope was 22" and 11" at 3 and 1.3 mm respectively. Pointing and focus were monitored regularly. Pointing corrections were always found to be smaller than 3". Calibration of the data was made by observing a hot and cold loads with known temperatures, and the line intensities were converted to main beam brightness temperature, $T_{\rm MB}$, using main beam efficiencies of 0.74 and 0.48 at 3 and 1.3 mm respectively. The spectra are shown in Fig 1c-d and the observed parameters as derived from Gaussian fits are listed in Table 2.

3. Analysis

In Fig. 2 we show the H_2 rotational diagrams for the two sources. The open squares correspond to the column densities as measured with ISO, without any correction for the different apertures in the different lines and for the dust extinction. The rotational diagrams for the two sources show a zig-zag distribution since the column densities in the ortho-H_2 levels J=3 and 5 are lower than those expected from the para-H_2 levels for the LTE OTPR. For the typical temperatures involved in these transitions ($\sim$ 200 K), the LTE OTPR is $\sim$ 3. Similar rotational diagrams derived from the H_2 pure-rotational lines have been previously found in HH54 by Neufeld et al. (1998) and in NGC7023 by Fuente et al. (1999). For these sources where extinction is known to be low, the immediate conclusion was that the OTPR was not in LTE.

The H_2 emission has been detected in all sources of our sample indicating that the H_2 emission in the GC must be relatively widespread and extended (Martín-Pintado et al. 1999b). This is also suggested from the measured linewidths of the H_2 lines (see Section 2). Anyhow, even in the extreme case that the H_2 emission were point-like, the corrections for the different apertures would be small and would not affect substantially the conclusions about the OTPR. For a point-like source the S(0) line will be more diluted than the S(1) and S(2) lines because of the larger beam (20" $\times$ 27" instead of 14" $\times$ 27"). The situation for the S(3) line will be the opposite since the aperture at this wavelength is 14" $\times$ 20". Therefore, in this limit case, the column densities in the level J=2 (derived from the S(0) line) averaged in a beam of 14" $\times$ 27" would be larger by a factor of 1.4, while on the opposite, the beam-averaged column density in the J=5 level would be smaller by a factor of 1.4. Hence, the correction for different apertures, cannot explain the zig-zag distribution in the rotational diagram.

A more critical correction is that for the extinction produced by the foreground material. As described by Martin-Pintado et al. (1999b) the weakness of the S(3) line in the GC clouds should be due to the extinction produced by the silicate feature at 9.7 μm in the foreground dust clouds. In clouds with a LTE H_2 OTPR, one can use the intensity of the S(3) line to estimate the visual extinction once the relative value for the opacity at 9.7 μm to the 0.55 μm opacity is known. One could, in principle, apply corrections for increasing extinctions until the column density in the J=5 level is consistent with the column densities derived for other levels, i.e., until the rotational plot is a straight line (in the case of a Boltzmann distribution with one source temperature) or a smooth curve (in the case of a temperature gradient). In clouds with a non-equilibrium OTPR one could use an equivalent method using only ortho-H_2 levels, but obviously more than two levels are needed. The effect of foreground extinction on the rotational diagram is illustrated in Fig. 2, where the observed fluxes have been corrected for 30 (filled triangles) and 60 mag (filled circles) of visual extinction, using the extinction law of Draine & Lee (1984). Visual extinctions larger than 60 mag are needed for consistency between the S(1) and S(3) line intensities and a LTE OTPR. In this case, the curvature of the rotational plots suggests the presence of a large temperature gradient in the H_2 emitting region. To constrain the visual extinction toward these sources, in the following sections we will estimate the total column densities of dust and gas from measurements of the continuum dust emission, ^{13}CO, and C^{18}O with a similar resolution to that of the SWS aperture.

3.1. H_2 column densities from C^{18}O and ^{13}CO observations

We applied the Large Velocity Gradient (LVG) approximation to our data, to derive the physical conditions and the column densities of molecular gas from the emission of the J=2-1 line of C^{18}O and the J=1-0 lines of C^{18}O and ^{13}CO. The lines toward the two sources show complex profiles with two velocity components. From the line intensity ratios one can see that these components have slightly different physical conditions. The C^{18}O J=2-1 to J=1-0 line ratio is 1.0-1.4 in M+3.06+0.34 and cannot be determined for the other source. The J=1-0 ^{13}CO to C^{18}O ratio ranges between 5 and 14 in M+3.06+0.34 and is > 7 in M+1.56−0.30. To within a factor of 2, these values are in agreement with the typical isotopic abundances found in the GC for carbon and oxygen (see Wilson & Matteucci 1994) indicating that the ^{13}CO lines are optically thin. From the C^{18}O J=2-1 to J=1-0 ratio we derive for M+3.06+0.34 the H_2 densities given in Table 3 for two cases: high kinetic temperature ($T_{\rm K}$=100 K) and low kinetic temperature ($T_{\rm K}$=20 K). For those H_2 densi-

ties we have constrained the total column densities using the ^{13}CO line intensities. When the C^{18}O lines were not detected the range of possible ^{13}CO(1-0) column densities was obtained by changing the H_2 density between 10^3 and 10^4 cm^{-3} for T_K=100 K and between $10^{3.5}$ and $10^{4.5}$ cm^{-3} for T_K= 20 K (see Hüttemeister et al. 1998). In the case of cold gas and even higher H_2 densities, the ^{13}CO column densities will increase only in a factor of 1.3 since for low temperatures and densities $\geq 10^4$ the J=1–0 transition of ^{13}CO is thermalized. The H_2 column densities, N_{H_2}, in Table 3 have been derived from the ^{13}CO column density and a fractional abundance with respect to H_2 of 5 10^{-6}. They are typically of a few 10^{22} cm^{-2}, in good agreement with the values given by Hüttemeister et al. (1998). With these column densities, we have derived the total visual extinction, A_v, using the standard conversion factor: N_{H_2}(cm^{-2})=A_v(mag) $\times$ 10^{21}. Thus the extinctions toward the two GC sources studied in this paper are typically of 15-20 magnitudes.

3.2. Dust column densities and temperatures

From the LWS data we can make a direct estimate of the dust temperature and the dust column densities toward both sources. Though the aperture of the LWS is larger than that of the SWS, the dust emission in the GC is relatively smooth (Odenwald & Fazio 1984) and one does not expect large variations within the LWS aperture. The spectra for the two sources have very similar shapes with the maximum of the emission at $\sim$ 100 μm, indicating that the bulk of the dust is relatively cold with temperatures below 30 K, in agreement with previous estimates (Odenwald & Fazio 1984; Gautier et al. 1984).

The data cannot be fitted with only one gray body. For simplicity, we have considered a model with two gray bodies of temperatures T_1 and T_2. The total flux, S_λ, is given by:

$$S_\lambda = \Omega[B(T_1,\lambda)(1-e^{-(1-f)\tau(\lambda)})+B(T_2,\lambda)(1-e^{-f\tau(\lambda)})] \quad (1)$$

where Ω is the solid angle of the continuum source, $B(T)$ is the Planck function, f is the fraction of the opacity due to the warmer component (T_2), and $\tau(\lambda)$ is the total opacity at wavelength λ. In this model, the ratio of the visual extinction, A_v, to the total optical depth at 30 μm is taken from the Draine & Lee (1984) extinction law and the opacity for $\lambda > 30$ is given by:

$$\tau(\lambda) = 0.014 A_v (30\mu\mathrm{m}/\lambda)^\alpha \quad (2)$$

where α is the spectral index of the dust emission. In accordance with previous estimates for the envelope of Sgr B2 (Martín-Pintado et al. 1990) and for the GC background of the cold core GCM 0.25+0.11 (Lis & Menten 1998), we have taken $\alpha \simeq 1$. We have assumed extended emission ($\Omega = \Omega_{LWS}$) and then we have fitted the continuum spectrum with f, A_v, T_1, and T_2 as free parameters. As an example, we show in Fig. 3 the best fit to the LWS spectra towards M+1.56−0.30 obtained with A_v=40, T_1=15 K, T_2=27 K and f=0.1.

Table 4 lists the results of the parameters for the best fits for the two sources. The visual extinctions derived for the two sources are 30 and 40 mag. These values are in agreement, to within a factor of 2, with those derived from the CO data.

The dust emission is dominated by the cool ($T \sim 15$ K) component ($\tau_{v_1} \sim (1-f)\tau_v$), while the slightly warmer component ($T \sim 30$ K) contributes only 10%-20% to the total optical depth ($\tau_{v_2} \sim f\tau_v$). We can also fit the spectra with larger spectral indexes by increasing the dust column densities. For instance, an spectral index of 1.5 will increase the visual extinction to 50-100 mag. These high values of A_v are very unlikely since they are almost one order of magnitude higher than the estimates made from CO (see Table 3).

Since the extinction derived from CO and the continuum accounts for the total gas and dust along the line of sight, they must represent an *upper* limit to the extinction to the H_2 emitting region. Considering the uncertainties introduced by the unknown spectral index and the many free parameters in the dust column density determination, in the following discussion we will assume that upper limits to the visual extinction of the H_2 emitting region are those derived from the CO emission, namely, 16 magnitudes for M+3.06+0.34 and 20 mag for M+1.56−0.30. These values are within a factor of two of estimates obtained from the total dust column density.

3.3. Warm H_2: ortho-to-para ratio and column densities.

As discussed at the beginning of Sect. 3 the H_2 OTPR depends on the correction for extinction. In the previous sections we have estimated the extinction for the two clouds and Fig 4 shows the H_2 rotational diagrams for M+3.06+0.34 and M+1.56−0.30 corrected for the estimated extinctions. The error bars take into account the errors in the Gaussian fits of the lines and the calibration uncertainties. From these data, we derive an *ortho rotational temperature*, T_o, from the ortho-H_2 levels J=3 and J=5. In the same way, one can define a *para rotational temperature*, T_p, derived from the para-H_2 levels J=2 and J=4, and an *ortho-para temperature*, T_{op}, derived from the ortho level J=3 and the para level J=2. These temperatures are listed in Table 5. As we see, T_p is $\sim$ 250 K for both sources while T_o is slightly higher ($\sim$ 270 K) indicating the presence of a moderate temperature gradient. This effect is more definite in other sources of our sample, where the S(4) and S(5) lines, which trace clearly higher temperatures, have also been observed (Martín-Pintado et al. 1999b). For the present sample, T_{op} is $\sim$ 160 K, much smaller than T_p and T_o indicating a non-LTE OTPR. In

terms of these temperatures, the OTPR measured from our data will be given by:

$$\mathrm{OTPR} = \mathrm{OTPR_{LTE}}(T_\mathrm{p}) \exp(\frac{1}{T_\mathrm{p}} - \frac{1}{T_\mathrm{op}}) \quad (3)$$

where $\mathrm{OTPR_{LTE}}$(T) is the LTE OTPR at temperature T. As mentioned before, $\mathrm{OTPR_{LTE}}$ is ~ 3 for $T \geq 200$ K. Using Eq. (3), one finds an OTPR of ~ 1 for both sources (see Table 5). Increasing the extinction will make the H_2 OTPR closer to the equilibrium value, however extinctions > 70 mag will be required to give an LTE OTPR ratio. Such large visual extinctions are very unlikely from the molecular line and continuum data discussed in the previous sections. We therefore conclude that for the two sources the H_2 OTPR is *not* in equilibrium. Since the estimated error is ~ 0.4, we can take ~ 1.4 as a conservative upper limit for the OTPR in these two sources.

Extrapolating the populations in the J=2 and J=3 levels to the J=0 and J=1 levels , respectively, as two different species at temperature T_p, one finds that the total column densities of warm H_2 are $\sim 2\ 10^{21}$ cm^{-2} . This must be considered as a *lower* limit to the actual warm H_2 column density since the populations of the lowest levels (J=0 and J=1) can be increased significantly by colder, though still warm ($\sim$ 100 K) gas. Of course, if extinction is higher column densities will also increase. This implies that the measured ratio of warm H_2 to cold gas traced by CO is at least 15%.

High gas kinetic temperatures in these two clouds are known to be present from the NH_3 observations of Hüttemeister et al. (1993). The rotational temperatures derived from the (4,4) and the (5,5) metastable inversion lines of NH_3 are in good agreement with the temperatures derived in this paper using the lowest H_2 pure-rotational lines. Extrapolating the populations in the (4,4) and the (5,5) NH_3 levels to lower levels with the rotational temperature derived for each source by Hüttemeister et al. (1993) one finds a column density of warm NH_3 of $\sim 7\ 10^{14}$ cm^{-2} in both sources. Taking into account the warm H_2 column densities given above, we find a NH_3 abundance of (2-4) 10^{-7}, similar to the value obtained by Martín-Pintado et al. (1999a) in the expanding shells of the envelope of Sgr B2. A similar abundance is also obtained when we compare the column densities of cold ($\sim$ 20 K) NH_3 (Hüttemeister et al. 1993) and the H_2 column densities derived by our ^{13}CO and C^{18}O data.

3.4. Warm dust column densities

If the gas and dust are coupled, one expects that the dust associated with the warm H_2 component would be an intense continuum emitter in the mid- and far-IR. There is no hint of such dust component in our data, as shown in Fig. 3, where we represent (as a dotted line) the emission of a gray body with a temperature of 250 K and the size of the SWS aperture attenuated by the total column density of the cold component. The equivalent H_2 column density of warm dust used to simulate the emission in Fig. 3 is only $5\ 10^{18}$ cm^{-2} . Even this small column density should have been detected. Hence, we can rule out a dust component coupled to the warm gas with a column density larger than $2\ 10^{-3}$ times that of the warm H_2. On the other hand, the comparison of CO emission with the cold dust emission shows agreement with the standard gas-to-dust ratio within a factor of two.

4. Discussion

4.1. Heating of the warm component

The large column densities of warm H_2 and the low column densities of associated warm dust require a heating mechanism that heats selectively the gas maintaining the dust at much lower temperatures. A PDR with an incident far-ultraviolet (FUV) flux G_0 of ~ 100 (measured in units of $1.6\ 10^{-3}$ ergs cm^{-2} s^{-1}) can heat the gas via photoelectric effect in the grains to temperatures of 100-200 K in the external layers of the cloud without heating the dust to temperatures above 30 K (see Hollenbach et al. 1991). However, the large gas phase NH_3 abundance, as derived in Sect. 3.3, is not possible in such a PDR scenario. The evaporation temperature of NH_3 is $\sim$ 75 K, therefore it cannot be evaporated from grain mantles at only 30 K. Even in the case that evaporation occurs, the UV radiation that heats the dust would destroy the fragile NH_3 molecule. This is the behavior found in NGC 7023 where the NH_3 abundance is $\sim 10^{-8}$ in the well shielded region and decreases by more than a factor of 30 towards the region where the UV radiation increases and the dust temperature is $\sim$ 70 K (Fuente et al. 1990).

Shocks have been invoked as an important heating mechanism for the GC clouds (Wilson et al. 1982; Martín-Pintado et al. 1997; Hüttemeister et al. 1998). In fact, M+1.56−0.30 belongs to the "l =1.°5-complex", where Hüttemeister et al. (1998) derived the highest SiO abundance within their sample, while the CS abundance (which traces all dense gas, not just the part that has been subjected to shocks) is not enhanced. They interpreted the SiO enhancement to be produced by large scale dynamic effects, proposing that in this complex, gas sprayed from the intersection of the x_1 and x_2 orbits is crashing into material that is still on x_1 orbits in the context of a bar morphology. In our sample, M+1.56−0.30 is also the source with the highest SiO to CS ratio. Furthermore, Dahmen et al. (1997), studying the HNCO emission in this region, found evidence for collisional excitation by shocks.

On the other hand, M+3.06+0.34 is located close to one of the CS cores detected by Stark & Bania (1986) in the "Clump 2" complex. These dense cores are gravitationally bound but most of the CO is emitted from the lower density gas, not bound to the cores. Stark & Bania (1986) suggested that this material is the result of tidal

stripping of the cores. It is definite that shocks can play a role to explain the large column densities of warm H_2 and the relatively large abundances of NH_3, as well as the high kinetic temperatures in these clouds. In addition, transient heating by shock waves provides a natural explanation for H_2 OTPRs out of equilibrium.

We have compared the results of the model calculations for slow shocks by Timmermann (1998) with our H_2 data. Interpolating the H_2 line strengths predicted by the model for a preshock OTPR=1 as a function of density, we found that a shock with velocity of 10 km s^{-1} and a preshock H_2 density of $\sim 2\ 10^5$ cm^{-3} reproduces the observed line intensities. The results are displayed in Fig. 5 in the form of rotational plots. Open squares are the predicted column densities, while filled circles are the values derived from observations after correcting for extinction. Though the observed flux in the S(0) seems to be slightly larger than in the model, the agreement is excellent, and calibration errors can account for the discrepancies. The preshock density seems somewhat high but it is plausible since the S(3) line is *apparently* thermalized, which implies a lower limit to the H_2 density of $\sim 10^4$ cm^{-3} . In any event, the widespread distribution of the HCN emission (Jackson et al. 1996) shows that densities of $\sim 10^5$ cm^{-3} are common in the GC.

4.2. The ortho-to-para ratio

The main processes that affect the OTPR of H_2 are proton exchange collisions with H^+ and reactive collisions with H atoms. Ortho-para conversion in grain surfaces is thought to be less efficient. The rate coefficient for the proton exchange reaction

$$H_2(\text{ortho}) + H^+ \rightleftharpoons H_2(\text{para}) + H^+ + 170.5\ \text{K} \qquad (4)$$

is $\sim 3\ 10^{-10}$ cm^3 s^{-1} (Gerlich 1990). The analogous reactions with H_3^+ and H_3O^+ may also occur at a similar rate (see e.g. Le Bourlot et al. 1999). This rate gives an ortho-para conversion timescale, $\tau_{\rm conv}$, of $\sim 100/n(^+)$ yr, where $n(^+)$ represent the density of H^+, H_3^+ or H_3O^+ in cm^{-3} . One should note that the actual conversion time can be a factor of 10 larger than $\tau_{\rm conv}$ (see Flower and Watt 1984).

The rate coefficient for the reactive collisions with H atoms

$$H_2(\text{ortho}) + H \rightleftharpoons H_2(\text{para}) + H + 170.5\ \text{K} \qquad (5)$$

is $\sim 8\ 10^{-11}\text{e}^{-(3900/T)}$ cm^3 s^{-1} (see e.g. Le Bourlot et al. 1999). Due to the high activation barrier of this reaction (3900 K), in cold and dense molecular clouds the dominant process will be proton exchange collisions. This is also true for low velocity shocks of ~ 10 km s^{-1} since the maximum temperature achieved in the post-shock region is only $\sim$ 300 K. If the H^+ and H_3^+ densities ($n(H^+)$, $n(H_3^+)$) in the postshock region of a 10 km s^{-1} shock were as high as $\sim 10^{-3}$ cm^{-3} (see Timmermann 1998), $\tau_{\rm conv}$ would be $\sim 10^5$ yr. It is worth-noting that recent models for ortho-para conversion in shocks by Wilgenbus et al. (2000) find much lower H^+ and H_3^+ densities in the postshock region. In this case, the timescale for ortho-para conversion would be $> 10^5$ yr. On the other hand, the time needed for the passage of the proposed 10 km s^{-1} velocity shock, from the point where the neutral gas starts to heat up to the point where the gas has reached interstellar temperatures again, is $\lesssim 10^4$ yr (see Timmermann 1998). However the timescales in which the neutral gas is at high temperatures are much shorter. Hence, if the initial OTPR was lower than 3, the heating-cooling of the gas is too fast for the OTPR to reach the equilibrium at the temperatures of the shocked material.

Shocks with velocities > 20 km s^{-1} heat the gas to temperatures > 700 K. Then, collisions with H would be the main ortho-to-para conversion mechanism, and indeed, the ortho-para conversion timescale would be low enough to obtain at least some conversion in the shock timescale as in the source HH54 (Neufeld et al. 1998). However, the lines ratios in M+1.56−0.30 and M+3.06+0.34 cannot be explained with a preshock OTPR of < 1 and a shock with velocity >10 km s^{-1}. Therefore, the observed OTPR in these clouds must be approximately the preshock OTPR. This conclusion is independent of any shock model since the low temperatures involved by a 10 km s^{-1} shock are not sufficient for the H_2-H reactive collisions to be effective and, even for the largest predicted H^+ and H_3^+ abundances, the proton exchange reactions are not fast enough to give ortho-para conversion in the shock timescale.

If the OTPR of the preshock gas was in equilibrium at the gas temperature, the temperature should be ~ 80 K. In this case, the preshock gas should have been already heated before the shock front compresses and heats the gas to 250 K. However, there is no strong reason to believe that the preshock OTPR should be in equilibrium at the preshock temperature. The H_2 molecule is formed mainly on the grain surfaces by a highly exothermic reaction. Thus, if it is rapidly ejected to gas phase the OTPR will be the typical OTPR at high temperature, i.e., 3. On the other hand, if it is not evaporated immediately from the grain there will be ortho-to-para conversion by collisions with radicals, impurities or defects and the OTPR could reach the equilibrium value at ~ 30 K (dust temperature) of $\sim$0.01. In our case, the preshock OTPR of ~ 1 suggests that the H_2 molecules were ejected from the grains with OTPR >1. Afterwards, this ratio could decrease due to proton exchange processes.

The equilibrium proton abundance in dense ($n(H_2)$ $\sim 10^5$ cm^{-3}) clouds, where photoprocesses are not important, depends mainly on the ionization by cosmic rays and on charge exchange reactions with neutral molecules. Modeling the chemistry of dense PDRs, Sternberg and Dalgarno (1995) found $n(H^+)$ of $\sim 10^{-5}$ cm^{-3} in the well UV-shielded region for a cosmic ray ionization rate (ζ) of

5 10^{-17}s^{-1}, implying $\tau_{\rm conv} \sim 10^7$ yr. A similar timescale is obtained for proton exchange collisions with H_3^+. The density of H_3O^+ could reach 10^{-4} cm^{-3} and thus $\tau_{\rm conv}$ could decrease by a factor of 10. Nevertheless, the actual time to reach the LTE OTPR would be longer. Flower & Watt (1984) have studied the temporal evolution of the OTPR in molecular clouds. Using the same rate coefficient as above for the proton exchange process, they have shown that for H^+ densities [2] of $10^{-4} - 10^{-5}$ cm^{-3} the actual time needed for an OTPR=3 to be in equilibrium at 30 K (similar to the observed cold component in the GC clouds) is $\sim 10^7 - 10^8$ yr. In particular, if $n(H^+)$ (or $n(H_3O^+)$) is $\sim 10^{-4}$ cm^{-3} , then $\sim$ 5 10^6 yr will be needed to have an OTPR=1. Assuming that the H_2 was ejected to gas phase after formation with an OTPR $\lesssim$3, the shock front reached the cloud approximately 10^6 yr after the formation of the H_2 molecules, since this is the time needed for an OTPR$\sim$3 to descend to $\sim$1 in a dense molecular cloud.

5. Conclusions

We have presented ISO SWS observations of the S(0), S(1), S(2), and S(3) pure-rotational lines of H_2 and LWS observations of the dust continuum and IRAM-30m ^{13}CO and C^{18}O observations toward the GC molecular clouds M+1.56−0.30 and M+3.06+0.34 . Using the CO data and dust column densities from the LWS spectra we estimate $\sim$ 20 mag of visual extinction toward these sources. The two estimates of the extinction agree within a factor of 2 for the standard gas-to-dust conversion factor. According to the two components scenario proposed by Hüttemeister et al. (1993), the low-J CO emission arises from the cold gas component and is coupled to the dust at a temperature of $<$ 30 K. The warm component ($T \sim 250$ K) column density observed directly in H_2 is, at least, $\sim$ 15 % of the cold one and would have very little warm dust associated with it. From the LWS spectra we set a conservative upper limit to the warm gas column density associated with the warm dust of 2 10^{-3} times that of the warm H_2 column density.

After correcting for the dust extinction, we derive an OTPR of 1.0 ± 0.4, which is far from the LTE value expected for the gas temperatures of 250 K. We have also compared the warm H_2 column densities to the NH_3 observations by Hüttemeister et al. (1993), and derived NH_3 abundances of $\sim$ 2 10^{-7}, similar to those in the cold component (Hüttemeister et al. 1993).

The low dust temperatures, the high NH_3 abundances, the large CO linewidths, the non-LTE H_2 OTPR, in addition to the high gas temperatures suggest that the warm gas component is heated by low velocity shocks with speeds of $\sim$ 10 km s^{-1} . To explain the OTPR we propose the following scenario. H_2 is formed in the grain surfaces and ejected to gas phase with OTPR$\lesssim$3. After $\sim 10^6$ years, the time required to reach the preshock OTPR=1, a low velocity shock heated the gas to the observed temperatures of 250 K, but the OTPR was almost unaltered because the timescale for the passage of such a shock is much shorter than the ortho-to-para conversion timescale. Taking into account the shock timescale this occurred less than 10^4 yr ago. It is interesting to note that the timescale of the cloud's galactic rotation period is also $\sim 10^6$ years. This fact suggests that the origin of the shocks can be related to large scale dynamics of the GC region.

Acknowledgements. We thank S. Cabrit for her helpful comments on the ortho-to-para conversion mechanisms. We acknowledge support from the ISO Spectrometer Data Center at MPE, funded by DARA under grant 50 QI 9402 3. NJR-F, JM-P, PdV, and AF have been partially supported by the CYCIT and the PNIE under grants PB96-104, 1FD97-1442 and ESP97-1490-E. NJR-F acknowledges *Conserjería de Educación y Cultura de la Comunidad de Madrid* for a pre-doctoral fellowship.

[2] In their model these proton densities were obtained with $\zeta = 10^{-17} - 10^{-18}$s^{-1} using a simplified chemical network.

References

Bally J., Stark A.A., Wilson R.W., 1988, ApJ 324, 223
Chrysostomou A., Brand P.W.J.L., Burton M.D., Moorhouse A., 1993, MNRAS 265, 329
Clegg P.E., et al., 1996, A&A 315, L38
Cox P., Laureijs R., 1989, IRAS Observations of the Galactic Center. in: Morris M. (ed.) Proc. IAU Symp. 136, The Center of the Galaxy. Kluwer, Dordrecht, p. 121
Dahmen G., Hüttemeister S., Duschl W.J., 1997, HNCO in the Galactic Center GMC G+1.6-0.025 -Evidence for collisional excitation by strong shocks. in: Sofue Y. (ed.) Proc. IAU Symp. 184, The Central Regions of the Galaxy and Galaxies. Kluwer, Dordrecht, p. 95
Draine B.T., Lee H.M., 1984, ApJ 285, 89
Flower D.R., Watt G.D., 1984, MNRAS 209, 25
Fuente A., Martín-Pintado J., Cernicharo J., Bachiller R., 1990, A&A 237, 471
Fuente A., Martín-Pintado J., Rodríguez-Fernández N.J., Rodríguez-Franco A., de Vicente, P., 1999, ApJ 518, L45
Gautier T.N., et al., 1984, ApJ 278, L57
Gerlich D., 1990, J. Chem. Phys. 92, 2377
de Graauw Th., et al., 1996, A&A 315, L49
Güsten R., Walmsley C.M., Pauls T., 1981, A&A 103, 197
Hollenbach D.J., Takahashi T., Tielens A.G.G.M., 1991, ApJ 377, 192
Hüttemeister S., Wilson T.L., Bania T.M., Martín-Pintado J., 1993, A&A 280, 255
Hüttemeister S., Dahmen G., Mauersberger R., Henkel C., Wilson T.L., Martín-Pintado J., 1998, A&A 334, 646
Jackson J.M., Heyer M.H., Paglione T.A.D., Bolatto A.D., 1996, ApJ 456, L91
Kessler M.F, et al., 1996, A&A 315, L27
Le Bourlot J., Pineau des Forêts G., Flower D.R., 1999, MNRAS 305, 802
Lis D.C., Menten K.M., 1998, ApJ 507, 794
Martín-Pintado J., de Vicente P., Wilson T.L., Johnston K.J., 1990, A&A 235, 193

Martín-Pintado J., de Vicente P., Fuente A., Planesas P., 1997, ApJ 482, L45
Martín-Pintado J., Gaume R.A., Rodríguez-Fernández N.J., de Vicente, P., Wilson T.L., 1999a, ApJ 519, 667
Martín-Pintado J., Rodríguez-Fernández N.J., de Vicente P., Fuente A., Wilson T.L., Hüttemeister S., Kunze D., 1999b, The Hot Gas and the Cold Dust in the Galactic Center as seen by ISO. in: Cox P., Kessler M. (eds.) The Universe as Seen by ISO. ESA, Noordwijk, SP-427, Vol. 2, p. 711
Mauersberger R., Henkel C., Wilson T.L., Walmsley C.M., 1986, A&A 162, 199
Morris M., Serabyn E., 1996, ARA&A 34, 645
Neufeld D.A., Melnick G.J., Harwit M., 1998, ApJ 506, L75
Odenwald S.F., Fazio G.G., 1984, ApJ 283, 601
Salama, A., et al., 1997, Topics in SWS Data Analysis and Calibrations. in : Heras A.M., Leech K., Trams N.R., Perry M. (eds.) First ISO Workshop on Analytical Spectroscopy. ESA, Noordwijk, SP-419, p. 17
Smith M.D., Davis C.J., Lioure A., 1997, A&A 327, 1206
Stark A.A., Bania T.M., 1986, ApJ 306, L17
Sternberg A., Dalgarno A., 1999, ApJS 99, 565
Sternberg A., Neufeld D.A., 1999, ApJ 516, 371
Swinyard B.M., et al., 1996, A&A 315, L43
Timmermann R., 1998, ApJ 498, 246
Valentijn E.A. et al., 1996, A&A 315, L60
Valentijn E.A., Van der Werf P.P., 1999, ApJ 522, L29
Wilgenbus D., Cabrit S., Pineau des Forêts G., Flower D.R., 2000, A&A, (submitted)
Wilson T.L., Ruf K., Walmsley C.M., Martin R.N., Pauls T.A., Batrla W., 1982, A&A 115, 185
Wilson T.L., Matteucci F., 1992, A&AR 4, 1

Table 3. Derived physical conditions for the ^{13}CO and C^{18}O lines for $T_{\rm K}$=20 K and $T_{\rm K}$=100 K

Source	$T_{\rm K}$ K	log(n$_{H_2}$) log(cm^{-3})	$N_{^{13}\rm CO}$ [b] 10^{16} cm^{-2}	$N_{\rm H_2}$ 10^{21} cm^{-2}
M+3.06+0.34	100	3-3.8	5.8-8	12-16
	20	>3.3	$\lesssim$8	$\lesssim$16
M+1.56−0.30	100	3-4[a]	2.8-10.2	5.7-20
	20	3.5-4.5[a]	2.8-8.1	5.6-16.2

[a] When C^{18}O is not detected, we have used, following Hüttemeister et al. (1998), $n_{\rm H_2} \sim 10^{3-4}$ cm^{-3} when $T_{\rm K}$=100 K and, $n_{\rm H_2} \sim 10^{3.5-4.5}$ cm^{-3} when $T_{\rm K}$=20 K.
[b] Contains the contribution from both velocity components. Dispersion in the column densities are due to errors from the Gaussians fits to the spectra.

Table 4. Parameters of the best fits to the LWS spectra with two gray bodies assuming α=1 and $\Omega = \Omega_{\rm LWS}$: Temperatures, ratio of the opacity in the warmer component to the total opacity, and total visual extinction. Numbers in parentheses are 1σ errors of the last significant digit.

Source	T_1	T_2	f	$A_{\rm v}$
M+3.06+0.34	14(4)	24(2)	0.2(2)	30(20)
M+1.56−0.30	15(4)	27(3)	0.1(1)	40(20)

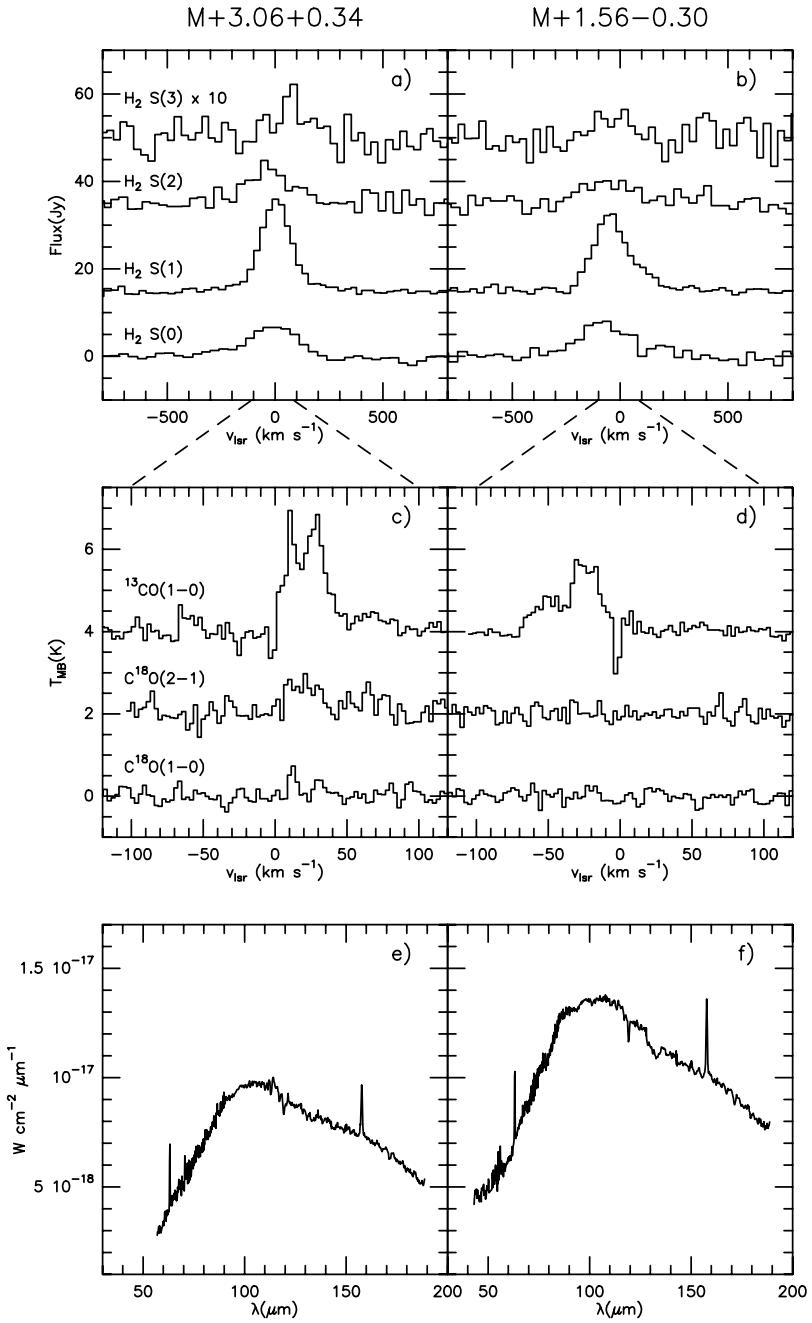

Fig. 1. Spectra of the two sources: **a-b** H_2 spectra taken with the SWS. **c-d** IRAM-30m spectra of the $C^{18}O$(1–0), ^{13}CO(1–0), and $C^{18}O$(2–1) lines. **e-f** LWS full grating spectra. Note the different radial velocities ranges in Fig. 1a-b and Fig. 1c-d.

Table 1. Observational parameters of the H_2 lines. Fluxes in units of 10^{-20} W cm^{-2} . Heliocentric velocities ($v_{\rm lsr}$) in km s^{-1}. Numbers in parenthesis are 1σ errors of the last significant digit of the Gaussian fits.

	S(0)		S(1)		S(2)		S(3)	
Wavelength	28.2μm		17.0μm		12.8μm		9.7μm	
Aperture	20" × 27"		14" × 27"		14" × 27"		14" × 20"	
	Flux	$v_{\rm lsr}$	Flux	$v_{\rm lsr}$	Flux	$v_{\rm lsr}$	Flux	$v_{\rm lsr}$
M+3.06+0.34	6.9(6)	-13(7)	19.6(6)	3(4)	16(3)	-30 (20)	1.6(5)	80(20)
M+1.56−0.30	8.1(9)	-80(10)	19(1)	-43(4)	14(3)	-50(20)	1.1(4)	-30(20)

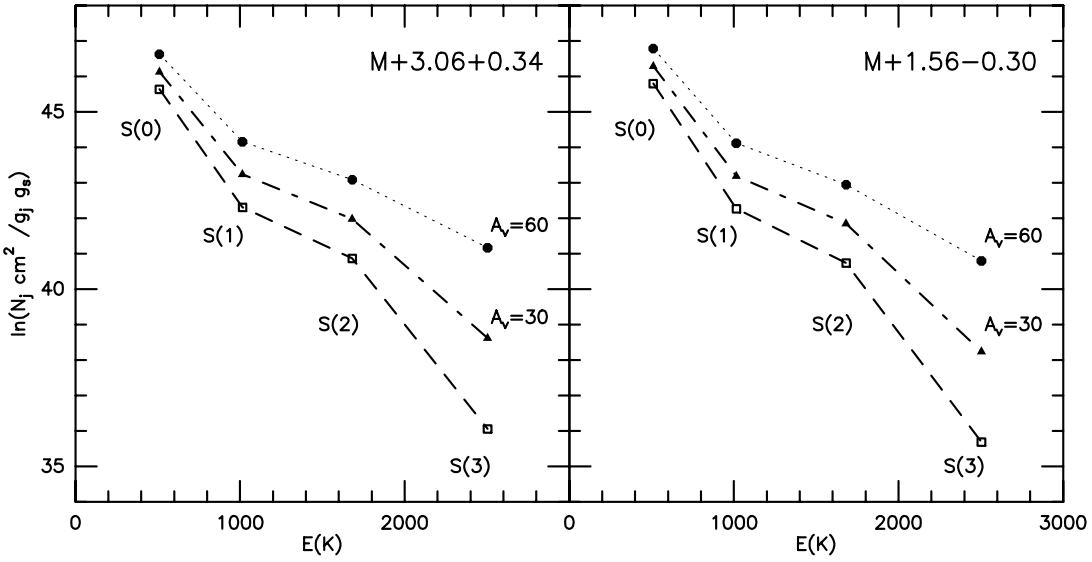

Fig. 2. Rotational plots. The results are displayed for three different values of the visual extinction: 0, 30, and 60 mag. We can see the typical zigzag distribution of a non-LTE OTPR. Extinctions higher than 60 mag are needed to have the smooth characteristic curve of emission arising from gas with an equilibrium OTPR and a temperature gradient.

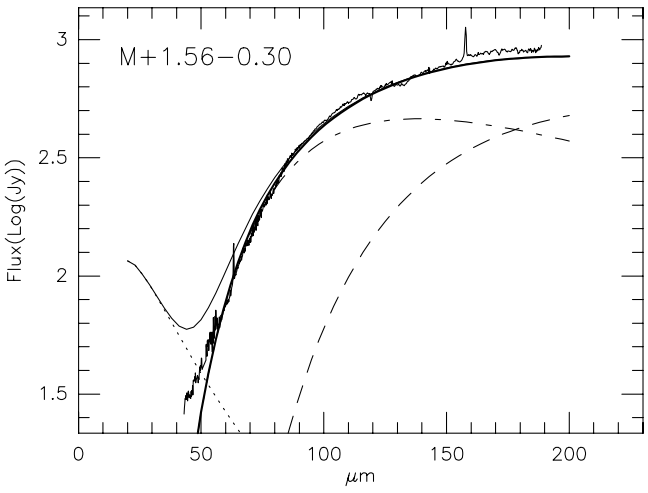

Fig. 3. The LWS spectrum of M+1.56−0.30 . The thick solid line is the best fit with two components of temperatures 15 K (dashed line) and 27 K (dot-dashed line). The solid line is the total emission for an equivalent column density of $N_{\rm H_2}$= 5×10^{18} cm^{-2} of hot (250 K) dust with $\Omega = 20" \times 20"$ (dotted line) located behind the cold dust. We have assumed that the hot component is extincted by the cold component.

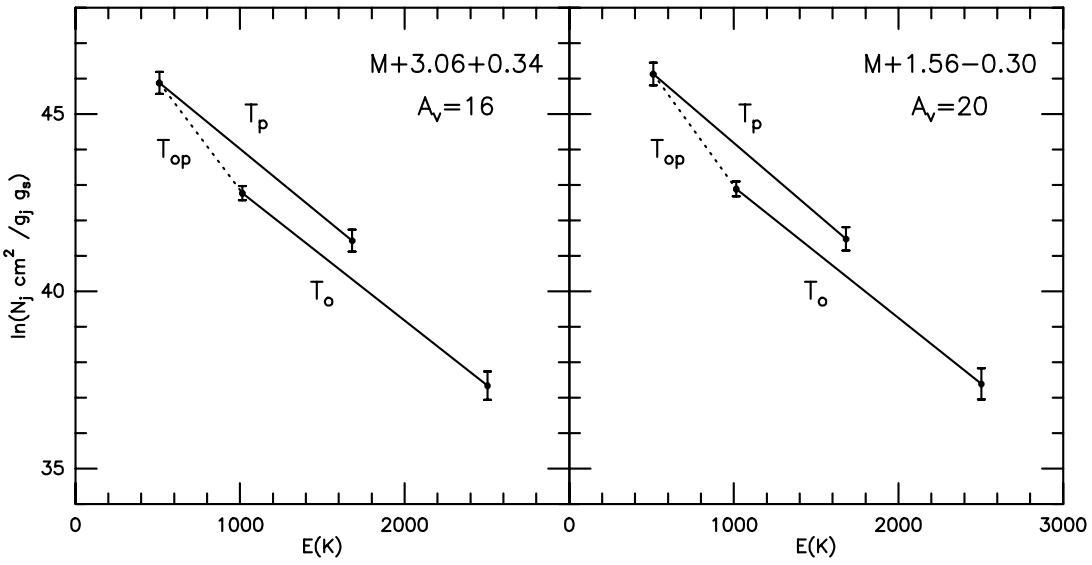

Fig. 4. Rotational plots after correcting for the most probable extinctions. The slope of the lines is proportional to the inverse of the temperature. $T_{\rm p}$ is the rotational temperature between the para-H_2 levels, $T_{\rm o}$ between the ortho-H_2 levels, and T_{op} between the ortho-level J=3 and the para-level J=2. Error bars take into account the calibration uncertainties and the errors in the Gaussian fits.

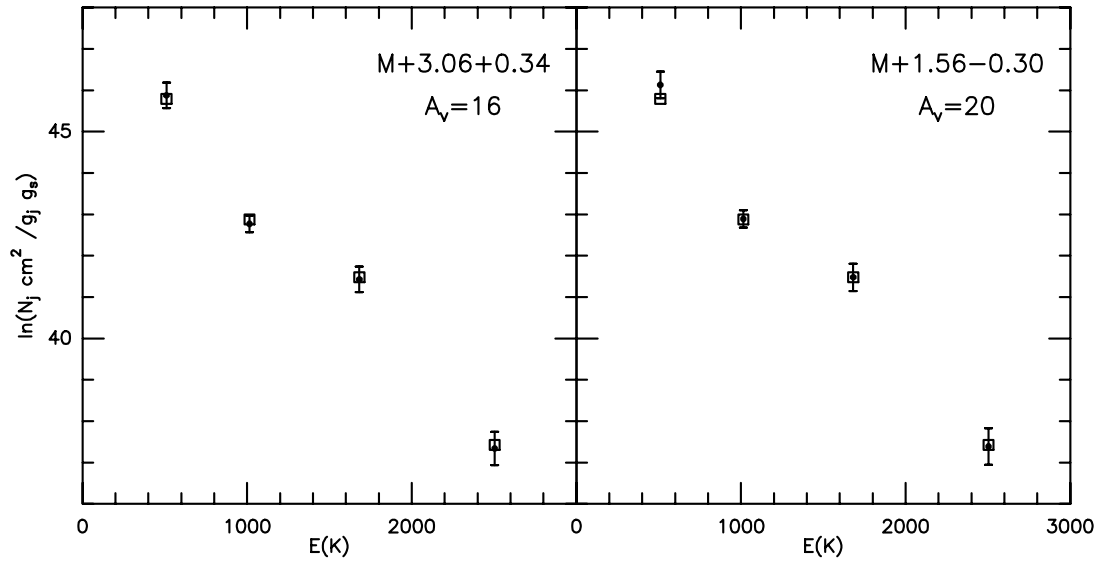

Fig. 5. Filled circles and error bars as in Fig. 4 Empty squares are the expected column densities using the model of Timmermann (1998) with preshock density $\sim 2\ 10^5$ cm^{-3} , shock velocity 10 km s^{-1} , and preshock OTPR=1

Table 2. Observational parameters of the $C^{18}O$ and ^{13}CO lines. Digits in parentheses are the errors in the last significant digits (rms of the Gaussian fits). For $C^{18}O(2–1)$ linewidths were fixed, when detected, to that of the $C^{18}O(1–0)$ lines.

Source	Position	$C^{18}O(1–0)^a$		$C^{18}O(2–1)^a$		$^{13}CO(1–0)$	
	$v_{\rm lsr}^{^{13}CO}$	Δv	$T_{\rm MB}$	Δv	$T_{\rm MB}$	Δv	$T_{\rm MB}$
	km s^{-1}	km s^{-1}	K	km s^{-1}	K	km s^{-1}	K
M+3.06+0.34	10.5(4)	6(1)	0.80(5)	6(0)	0.8(2)	10(1)	2.3(2)
	27.9(6)	8(3)	0.44(5)	8(0)	0.6(2)	18(2)	2.6(2)
M+1.56−0.30	-51(1)	—	≤0.14	—	≤0.20	19(5)	0.8(4)
	-24.1(6)	—	≤0.14	—	≤0.20	21(1)	1.8(4)

[a] Limits are 3σ assuming the same Δv than that for the ^{13}CO.

Table 5. Para, ortho, and ortho-para rotational temperatures, OTPR and H_2 column densities. Numbers in parentheses are 1σ errors.

Source	$T_{\rm p}$ (K)	$T_{\rm o}$ (K)	$T_{\rm op}$ (K)	OTPR	$N_{\rm H_2}$ (10^{21} cm^{-2})
M+3.06+0.34	260(30)	280(20)	160(20)	0.9(0.4)	2.6(1.0)
M+1.56−0.30	250(20)	270(20)	160(20)	1.0(0.4)	2.1(0.8)